Experimental Validation of Nozzle Flow Simulations for Rotating Detonation Rocket Engines

Alexis J. Harroun*, Stephen D. Heister†
Purdue University, West Lafayette, IN, 47907

and

Joseph H. Ruf‡
NASA Marshall Space Flight Center, Huntsville, AL, 35812

Rotating detonation engines (RDEs) promise increased thermodynamic performance that may significantly enhance the capabilities of current rocket platforms. Little work has been conducted thus far to characterize the effect of nozzle design on high chamber pressure RDEs. Previous computational work was completed to understand the nozzle performance of the Purdue methane/oxygen rocket RDE. A new experimental study on a similar kerosene/oxygen RDE was conducted to validate the results of the computational study. Both a nozzleless geometry and several aerospike designs were hot-fire tested. New pressure instrumentation on the different nozzle surfaces were included to better understand the flow physics unique to RDE chamber exit conditions. Both the previous computational study and the new experimental results confirmed that for a nozzleless geometry, the RDE cycle enhances suction on the base region, an important result to determining RDE engine performance separate from nozzle effects. While the aerospike experiments showed agreement with computational results, delay of flow separation due to the RDE cycle could not be confirmed. Two aerospike geometries with different nozzle pressure ratios were experimentally evaluated. This study showed both the strength and the necessity for 3D transient computations to better understand the RDE flow field with nozzle geometries.

I. Nomenclature

$CTAP$	=	capillary tube average pressure [atm]
f	=	frequency [Hz]
L	=	length [cm]
NPR	=	nozzle pressure ratio
P	=	pressure [atm]
P_a	=	ambient pressure [atm]
P_b	=	base pressure [atm]
P_c	=	chamber pressure [atm]
R	=	radial distance [cm]
t	=	time [s]
θ	=	azimuthal location [deg]

* Graduate Student, School of Aeronautics and Astronautics, AIAA Student Member.
† Raisbeck Engineering Distinguished Professor for Engineering and Technology Integration, School of Aeronautics and Astronautics, AIAA Fellow.
‡ Aerospace Engineer, ER42/Fluid Dynamics Branch, AIAA Member.

II. Introduction

Rotating detonation engines (RDEs) are an engine platform that employs constant-volume combustion to achieve higher theoretical thermodynamic efficiencies compared to current Brayton cycle-based rocket combustor designs. These thermodynamic benefits may translate to significant increases in possible payload capacities for launch vehicles or higher performance for space engines [1]. One of the least understood portions of the constant-volume cycle for an RDE is the expansion of the transient, high pressure ratio post-detonation gases exiting the combustor. Although nozzle design is well understood for constant pressure engines exhausting to changing ambient pressure conditions, the unique pressure field of an RDE presents especial challenges to employing even the one-dimensional analysis for typical de Laval nozzles. At present, computational methods and experiments must be used to determine the flow field exiting the combustor and expanding within a chosen nozzle geometry.

Most RDE experimental testing is performed without a nozzle to isolate the performance of the combustor from the downstream expansion surfaces. Typical RDE topologies utilize a centerbody to create an annular combustor geometry for the rotating detonation wave, which necessitates that a base region is formed at the aft end of the centerbody. Despite the effort to isolate the combustor performance, the base region will produce non-negligible base drag that is difficult to predict and must be estimated with CFD or directly measured. A better understanding of the pressure field produced on the base region is essential for more accurate experimental engine analysis.

The use of aerospike geometries for RDEs is of particular interest because they are designed to expand efficiently to changing chamber-to-ambient pressure ratio conditions. A zero-dimensional theoretical analysis of rocket RDEs at a wide range of operating conditions characterized the performance benefit of using a generic aerospike design over a typical bell nozzle at 2-5% [2]. Aerospike design for constant nozzle pressure ratios has been studied in detail [3-5]; however, the fact that RDEs exhaust gases are near or past their sonic point and have a wide range of pressure ratios that change in time makes designing a fixed aerospike geometry challenging. Few aerospike designs for rocket application – i.e., high average chamber pressure -- RDEs have been investigated in the literature. One experimental study showed utilizing a conical aerospike nozzle enhanced thrust over no nozzle by 6-10% [6], but did not perform more detailed analysis of the flow field physics. More work is required to understand how the RDE flow field interacts with the nozzle design and how this design can be tuned to exploit the enhanced work output of the constant-volume cycle.

The purpose of this study is to investigate two families of expansion geometries for an RDE: nozzleless and aerospike configurations. The nozzleless geometry is studied to determine the true effect of base drag on performance of an RDE so more accurate combustion efficiencies may be determined. Several aerospike geometries are investigated to determine their effect on RDE performance and how their geometries could be optimized. The first part of the broader study was a computational study based on previous experimental work [7]. This paper details the second part of this study, which aims to validate the computational study with new experimental testing.

A. Purdue Rocket RDE V1.3 Test Campaign

The Purdue Rocket RDE V1.3 test campaign was conducted by Stechmann in the spring of 2017 [8]. The V1.3 campaign tested an RDE with gaseous natural gas or methane and gaseous oxygen produced via a preburner configuration. Two nozzle geometries were investigated: a “nozzleless” geometry, where no expansion surfaces were used downstream of the engine exit, and an internal-external expansion (IE-) aerospike geometry (Fig. 1). The IE-aerospike geometry initially expands and redirects the flow toward the engine centerline within a cowl geometry before finishing the expansion externally. The IE-aerospike shown in Fig. 1 was designed by Stechmann for a nozzle pressure ratio (NPR) of 13.7 [1].

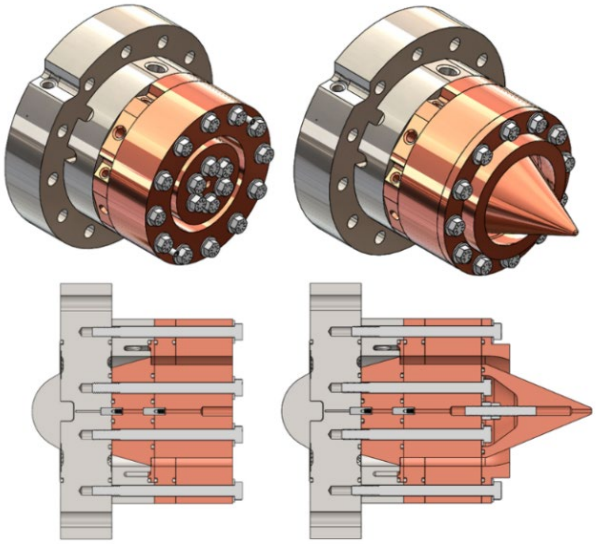

Fig. 1 Isometric and cross-sectional views of nozzle-less (left) and IE-aerospike (right) geometries for Purdue rocket RDE V1.3 test campaign. [8]

The computational portion of this study was conducted based on the experimental conditions from the V1.3 test campaign [8]. In particular, the inflow conditions for Test #53, which detonated gaseous methane and gaseous oxygen, were used because of its detonation stability and high performance. The inflow and performance parameters for Test #53 are shown in Table 1. Because it is impossible to directly measure chamber pressure in the chamber with high frequency instrumentation, a capillary-tube average pressure (CTAP) measurement taken near the injection site is used to estimate the average chamber pressure. The wave speed to Chapman Jouget (CJ) velocity ratio is a measure of the efficiency of the detonation wave and is used to estimate the attenuation from the theoretical detonation pressure ratio.

Table 1 Purdue Rocket RDE Test #53 Conditions

Propellants	Natural Gas & Oxygen
O:F Ratio	3.89
Total Mass Flow	1.15 [kg/s]
CTAP	8.6 [atm]
Thrust	2.3 [kN]
Wave Speed/CJ Velocity	88%
Wave Number	2
Frequency	13800 [Hz]

B. Purdue Rocket RDE V1.4 Test Campaign

The Purdue Rocket RDE V1.4 test campaign was led by Humble and Lim in the spring of 2019 [9]. While the basic configuration of the hardware was similar to the V1.3 campaign, the fuel investigated was liquid kerosene. In this test campaign, three nozzle configurations were tested. The nozzleless and IE-aerospike geometries were the same as the V1.3 hardware. Additionally, a flared aerospike geometry was also tested. In contrast to the IE-aerospike, the cowl "flares" away from the engine centerline so the supersonic flow exiting the chamber is not turned internally. The flared aerospike geometry was chosen to prevent possible recompression within the cowled region and to investigate higher area ratio nozzle designs. Figure 2 compares the geometry from the IE- and flared aerospike geometries. The flared aerospike was designed with the NASA Aerospike Design and Performance Tool (ADAPT) [10]. It was created with a design NPR of 19.3.

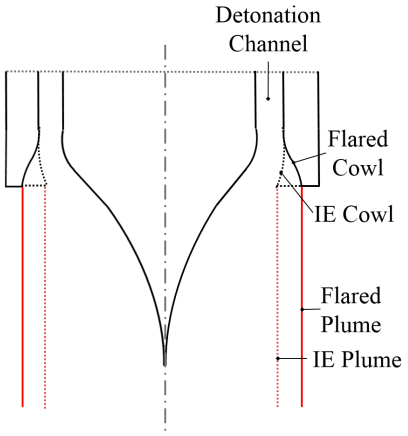

Fig. 2 Cross-sectional view of internal-external (IE) and flared aerospike designs. Dashed lines denote IE cowl and plume boundary at the optimal NPR while solid lines denote flared cowl and plume.

III. Methodology

A. Computational Modeling

As stated above, the computational portion of this study was based on the RDE V1.3 experimental conditions. To simplify the calculation, it was decided not to model the full combustion physics of the rotating detonation wave; instead, an inlet boundary condition to the domain was analytically developed based on the parameters in Table 1 and using a detonation case in NASA Chemical Equilibrium with Applications (CEA) [11]. A previous 2D unwrapped simulation by Mikoshiba was used to estimate the waveform of the pressure behind the detonation wave as a logarithmic decaying curve [12]. The CTAP and the detonation pressure ratio determined from NASA CEA results for methane and oxygen,were used to determine the bounds of the pressure waveform. This waveform was applied to the nozzle inlet boundary and "rotates" around the annulus azimuthally over time. The waveform as a function of time for a specific azimuthal location or azimuthal location for a specific time is defined by the following equations and is shown graphically in Fig. 3. The product species of the methane/oxygen detonation were used as the incoming nozzle species. The products were assumed to be frozen and chemical kinetics were ignored.

$$P(t) = -630000\ln(t) - 5780000\ [Pa] \tag{1}$$

$$P(\theta) = -630000\ln\left(\frac{\theta}{180} * \frac{1}{f}\right) - 5780000\ [Pa] \tag{2}$$

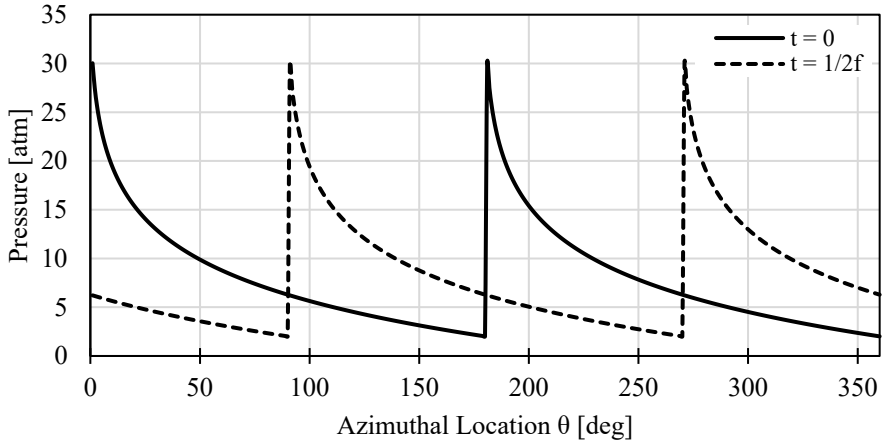

Fig. 3 Analytically-derived pressure waveform for Test #53 two-wave detonation at two different times.

Loci/CHEM, developed by Dr. Ed Luke at Mississippi State University [13], was the computational software used for this study. This code is a fully-implicit, dual time solver with 2nd order accuracy in both time and space. After a parametric study comparing turbulence models, the Mentor baseline (BSL) two-equation turbulence model with the Sarkar* compressibility correction [14] was chosen.

A cross-sectional view of the 3D computational domain for the IE-aerospike geometry is shown in Fig. 4. The boundary conditions are similar for the nozzleless geometry. The nozzle inlet is the boundary where the analytical detonation pressure wave, described above, was imposed. A quiescent inlet with a low flow velocity was used to simulate the entrained flow from the ambient air. The outlet was set to sea level ambient conditions. A quadrilateral mesh was employed to capture the boundary layer and turbulence flow physics near the engine and a portion of the exhaust plume. In the far-field, an unstructured tetrahedral mesh was used to reduce the cell count. A mesh convergence study was conducted for all geometries by doubly refining an axisymmetric mesh.

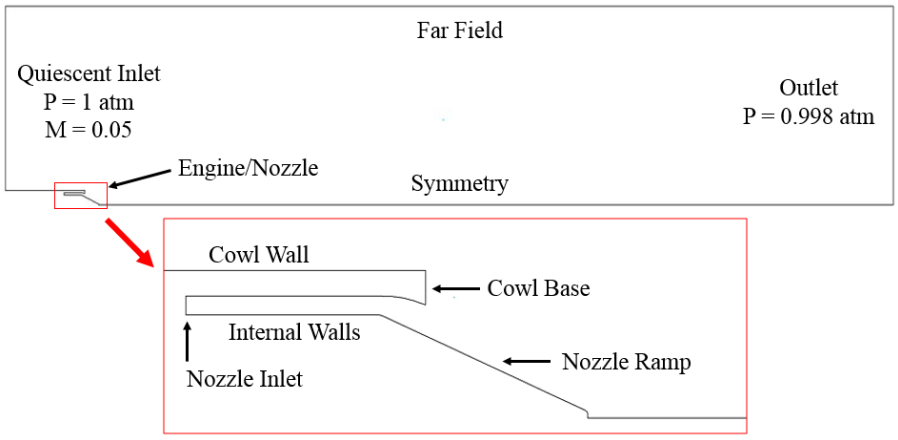

Fig. 4 Cross-sectional view of computational domain for RDE with IE-aerospike.

For this paper, only the results of the full three-dimensional computations with the temporal and spatially evolving inflow boundary condition are considered. These are the computational results that most closely resemble actual engine experimental conditions, with the caveat that the inflow conditions are based on the analytical inflow model.

B. Experimental Set-up

The V1.4 test campaign was partly designed to validate the computational results based on the V1.3 test campaign. In particular, pressure port instrumentation was added to allow direct measurement of the average steady-state pressures on the nozzleless base region and the aerospike plug surfaces. Although the V1.4 campaign used liquid kerosene instead of gaseous methane as its fuel, due to the difficulty of modeling liquid kerosene detonation in programs such as NASA CEA, it was decided to use the kerosene-based experimental results to validate the methane-based computational results. The ratio of specific heats for the constant pressure combustion of both propellants with oxygen is approximately the same, which gives confidence that the gas dynamics are relatively similar in both cases.

Seven base pressure measurements were included in the nozzleless configuration. Figure 5 shows a cross-section of the engine assembly hardware with the flow path of the pressure ports from the sampling locations to the pressure transducer mounting locations. Although the flow path is considerably long, based on testing, the pressures were able to rise to steady-state values during even the short sub-1 second duration of the hot-fire tests. Figure 5 shows the radial locations of the pressure measurements on the nozzleless base region. One measurement was at the centerline of the engine. The other six pressure ports were spaced evenly along the radius of the centerbody.

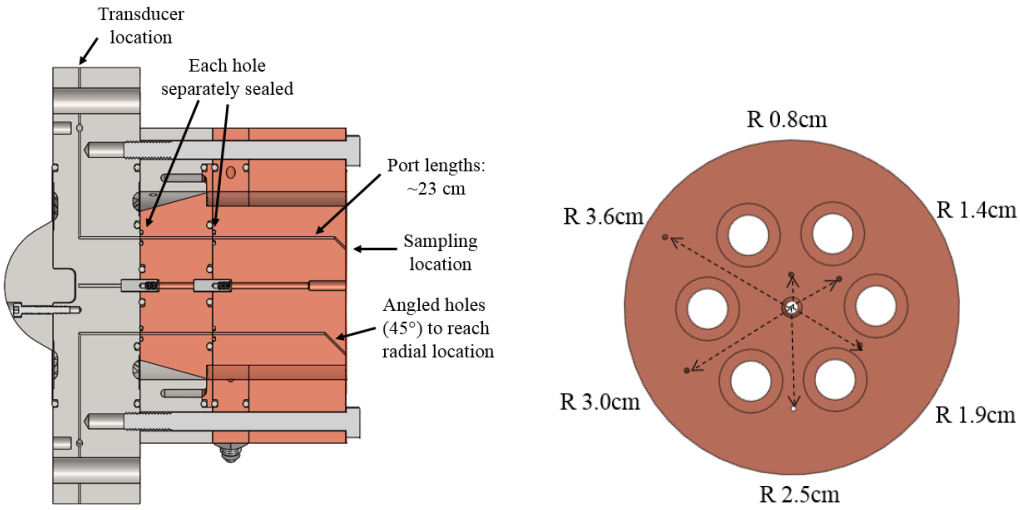

Fig. 5 Cut-away and front views of nozzleless configuration with pressure ports on base surface.

Six plug surface pressure measurements were included in the aerospike configuration. The plug geometry was shared between the IE- and flared aerospike configurations; only the cowl geometry was changed. Figure 6 shows a cross-section of the engine assembly hardware with the flow path of the pressure ports from the sampling locations to the pressure transducer mounting locations. Similar to the nozzleless configuration, the pressures were able to reach steady-state values during the duration of the hot-fire tests. Figure 6 shows the longitudinal locations of the pressure measurements on the aerospike plug surface. The pressure ports were spaced evenly along the length of the nozzle.

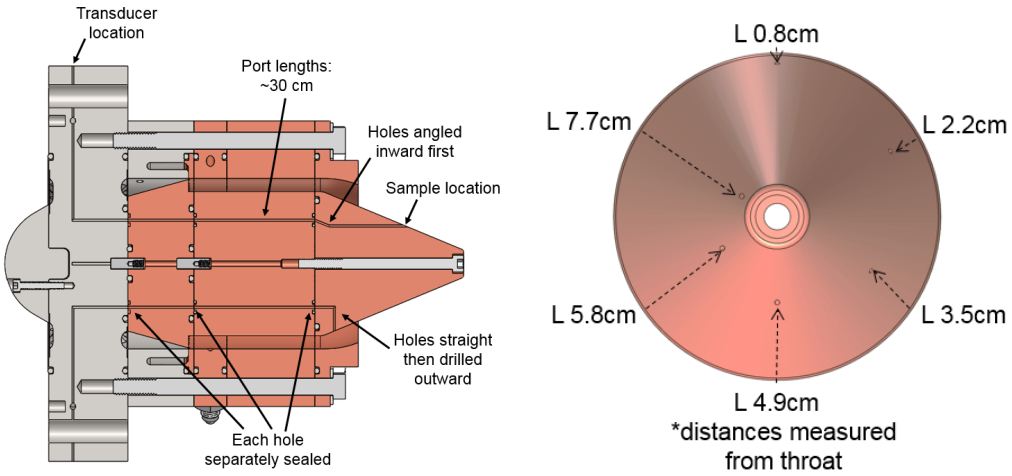

Fig. 6 Cut-away of aerospike nozzle configuration with pressure ports on ramp surface.

IV. Results

A. Nozzleless Base Pressures

1. Comparison of Computational Study to Experimental Results

Twenty-three tests with the nozzleless geometry were conducted at various inflow conditions in the V1.4 test campaign. Tests #54, 55, 65, 66, and 79 of the V1.4 campaign were compared to the computational results from the V1.3 campaign. The mass flow rates for these tests varied from 1.23 to 1.26 kg/s, a maximum 1% deviation from the 1.24 kg/s used in the V1.3 computation. The base pressure with radial distance for the V1.3 computation (dashed line) is compared to the discretized pressure measurements from the five V1.4 tests in Fig. 7. Although the propellants used were different, the test measurements agree well with the computational results. The surface-area averaged base

pressures for the tests varied from 0.58 to 0.60 psia, a 1% difference from the computational result. It should be noted that the pressure transducers used for stations 2-5 were different than those for 1-2 and 6-7, resulting in higher uncertainties noted in the figure.

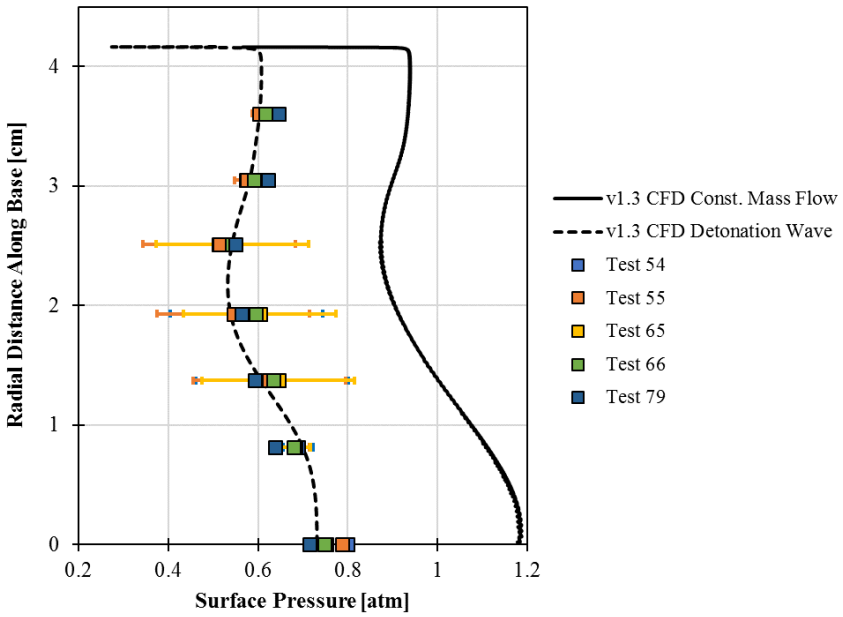

Fig. 7 Base pressure plots for V1.3 computations, including results from constant mass flow case and detonation wave case, compared to experimental results from V1.4 Tests #54, 55, 65, 66, and 79 for nozzleless geometry.

The computational result for a constant chamber pressure inlet boundary with the same mass flow rate (1.24 kg/s) is also plotted in Fig. 7 (solid line). Both the detonation wave computation based on the V1.3 campaign and the V1.4 test results confirm that the base pressures are significantly lower than expected for a constant chamber pressure engine. Previous analysis of the detonation wave computation [7] shows that the changing pressure field exiting the combustor effectively acts as an ejector, enhancing the pumping action on the base region. This leads to increased suction force on the base region and thus higher base drag for the RDE cycle versus constant pressure engines.

2. Open- versus Closed-Wake Behavior

Unfortunately, at present there is no way to create an analytical model predicting the base pressure – and thus the base drag – with respect to the operating conditions. Figure 8 demonstrates the non-linear relationship of the surface area averaged base pressure for the V1.4 tests with changing mass flow. An analytical model developed by Stechmann [8] to predict base pressure with changing mass flow rate is also plotted. The mid-range mass flow rate cases are sufficiently predicted by the linear model; at higher mass flow rates, however, the physics in the base region changes drastically, limiting the applicability of the model.

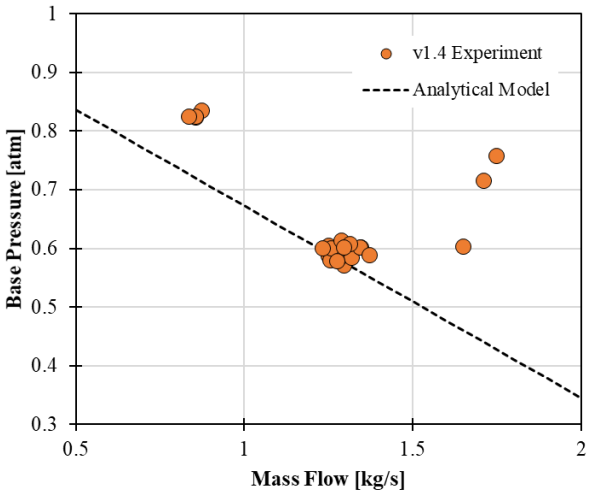

Fig. 8 Base pressure as function of incoming mass flow for V1.4 nozzleless experiments. Compared to Stechmann's analytical model. [8]

Literature of aerospike nozzle experiments with significantly truncated base regions has identified the emergence of different flow physics with respect to the chamber-to-ambient pressure ratio [15-16]. At low chamber-to-ambient pressure ratios, the region behind the base region is in "open-wake" mode, where the pressure will adjust to the ambient pressure. Once the chamber-to-ambient pressure ratio is high enough, the pressure in the base region will become independent of the ambient pressure: "closed-wake" mode. In Fig. 9, the ambient-to-chamber pressure ratio versus the ambient-to-chamber pressure ratio for the nozzleless V1.4 tests at various inflow conditions shows evidence of open- and closed-wake modes occurring. At the low chamber pressures tested (high ambient-to-chamber pressure ratios in the figure), the base pressure appears to adjust to the ambient pressure. At a certain pressure ratio, approximately $P_a/P_c = 0.15$, the base pressure becomes independent of the ambient pressure. More experiments would be required to further discretize this trend and determine the specific open- to closed-wake transition point. Literature of constant pressure aerospike engines has shown that the base pressure in open-wake mode will directly adjust to the ambient pressure, shown as the dotted $P_b/P_a = 1$ line in Fig. 9 [15-16]. In the RDE experiments, however, we see evidence that while the base pressure will adjust to the ambient pressure in open-wake mode, it will still be suctioned lower than the ambient pressure, which is further evidence to support the ejection mechanism the RDE performs on the base region.

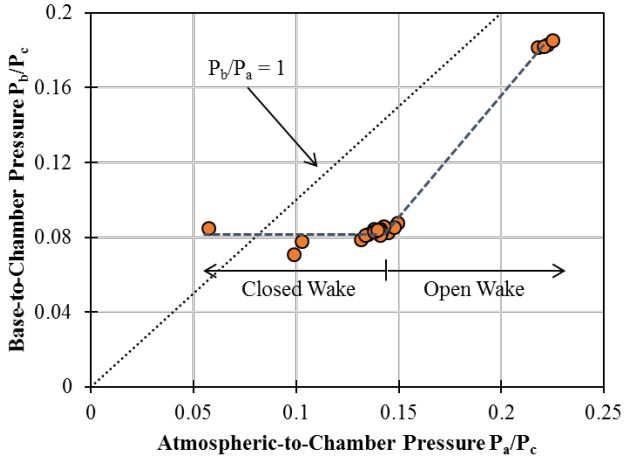

Fig. 9 Normalized base-to-ambient pressure for V1.4 nozzleless experiments. Open- to closed-wake transition at approximately $P_a/P_c = 0.15$.

B. IE-Aerospike Surface Pressures

Eight tests with the IE-aerospike geometry were conducted at various inflow conditions in the V1.4 test campaign. Tests #69, 70, and 77 of the V1.4 campaign were compared to the computational results from the V1.3 campaign. The mass flow rates for these tests varied from 1.27 to 1.32 kg/s, a 2-6% deviation from the 1.24 kg/s used in the V1.3 computation. The ramp surface pressure with radial distance for the V1.3 computation (dashed line) is compared to the discretized pressure measurements from the three V1.4 tests in Fig. 10. Again, although the propellants used were different, the test measurements agree reasonably well with the computational results. It should be noted that the pressure transducers used for stations 2-5 were different than those for 1-2 and 6, resulting in higher uncertainty.

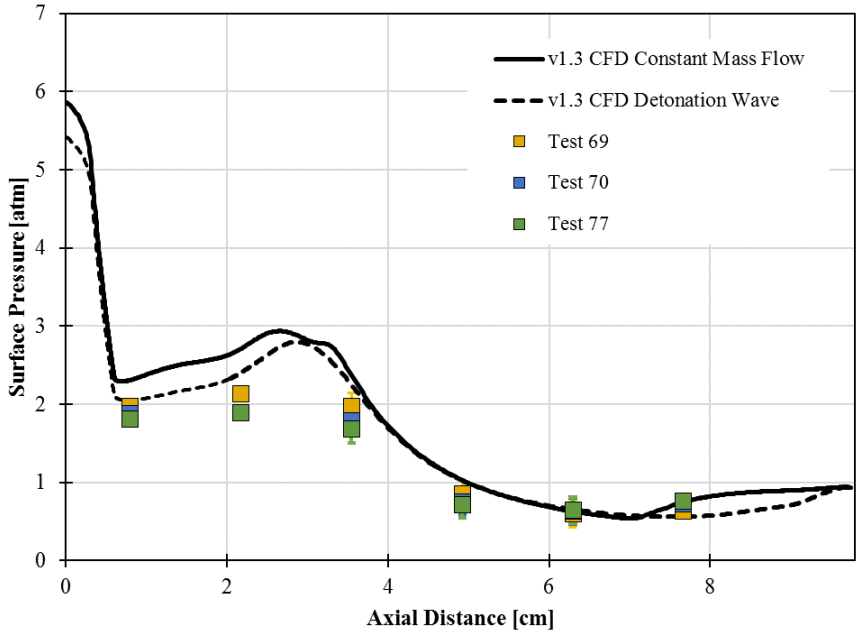

Fig. 10 Surface pressure plots for V1.3 computations, including results from constant mass flow case and detonation wave case, compared to experimental results from V1.4 Tests #69, 70, and 77 for IE-aerospike geometry. Cowl exit plane at 2.5 cm.

The computational result for a constant chamber pressure inlet boundary with the same mass flow rate (1.24 kg/s) is also plotted in Fig. 10 (solid line). A major finding from the computational study was the difference in the surface pressure contour between the constant chamber pressure and detonation wave cases; specifically, the detonation wave case showed a delay in flow separation at the end of the ramp [7]. Similar to the ejection action seen in the nozzleless case, the constantly re-pressurizing flow of the RDE re-energized the boundary layer at the end of the ramp, which kept the flow from separating. Unfortunately, there was not enough resolution in the experimental pressure port locations to be able to confirm this trend. Further studies with better pressure port resolution would be required to make a determination of the flow physics in this region.

C. IE-Aerospike versus Flared Aerospike Experiments

Three paired aerospike tests were performed at the same inflow conditions in the V1.4 test campaign. For each inflow condition, the test was performed first with either the IE- or flared aerospike cowl, and then another test with the other aerospike cowl was immediately performed with the same inflow condition. Again, the aerospike plug was kept the same for both configurations. Table 2 compares the inflow conditions for each paired aerospike test.

Table 2 Conditions for low-, mid-, and high-pressure paired tests for IE- and flared aerospike geometries.

	IE-Aerospike			Flared Aerospike		
Case	**Test #**	**CTAP [atm]**	**Mass Flow [kg/s]**	**Test #**	**CTAP [atm]**	**Mass Flow [kg/s]**
Low-Pressure	77	7.8	1.32	76	7.4	1.32
Mid-Pressure	73	8.3	1.45	75	8.5	1.48
High-Pressure	87	16.5	2.77	86	15.7	2.79

Fig. 11 shows the chamber pressure normalized surface pressures with respect to axial location for each aerospike design at a low-, medium-, and high-chamber pressure operating condition. The surface pressures are normalized to their respective chamber pressures to account for small changes in chamber pressure between each test. In all cases, the higher NPR flared aerospike design expanded the flow more quickly than the lower NPR IE-aerospike design, as indicated by the lower surface pressures. This trend suggests that for the pressure ratios tested, the IE-aerospike produces more pressure thrust. Unfortunately, the test campaign could not test higher pressure ratios better suited to the high NPR design of the flared aerospike because of a significant increase in heat loading and hardware destruction.

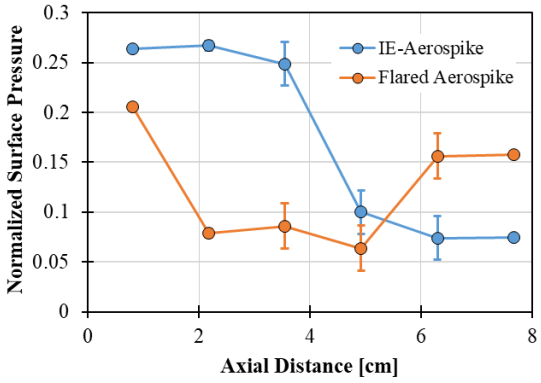

(a) Low-Pressure

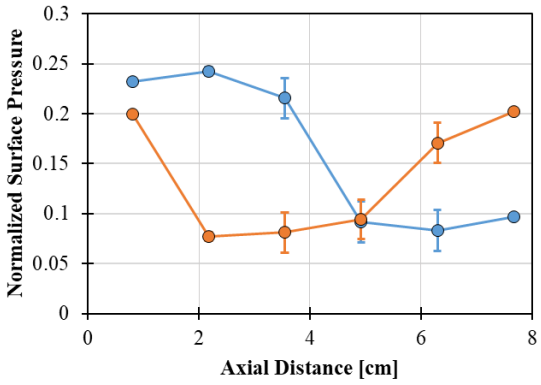

(b) Mid-Pressure

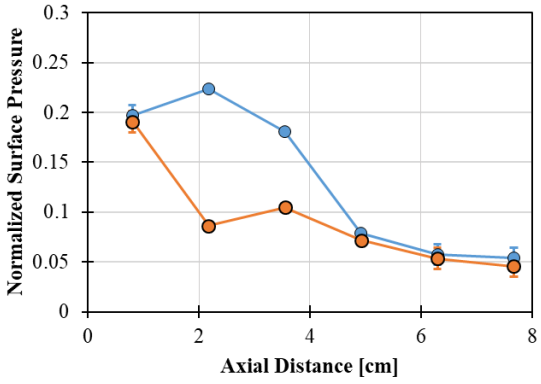

(c) High-Pressure

Fig. 11 Chamber pressure normalized surface pressures for IE- and flared aerospike geometries for (a) low- (b) mid- and (c) high-pressure inflow conditions.

It should be noted that the computational study did not investigate the flared aerospike geometry beyond 2D axisymmetric cases because of the long computation times associated with the full 3D transient boundary condition.

However, previous work using cycle-averaging of 2D axisymmetric constant pressure cases for both the IE- and flared aerospike geometries estimated that the flared aerospike geometry would produce 1% more specific impulse at pressure ratios near the investigated mid-pressure ratio paired V1.4 test [7]. The discrepancy suggests that either the computation is not capturing all of the flow physics present in the experiment or that the axisymmetric cycle-averaging is too simplistic of a method to estimating performance potential.

V. Conclusions

The results of a computational study based on the Purdue Rocket RDE V1.3 test campaign were compared to new experimental results from the Purdue Rocket RDE V1.4 test campaign. The V1.4 test campaign was designed with enhanced nozzle diagnostics to allow a better understanding of the flow physics for both nozzleless and aerospike nozzle geometries. The following major results were obtained:

1. Experiments confirmed the ejector action of the RDE cycle that enhances the base drag on the centerbody of an annular nozzleless RDE design beyond that predicted by constant pressure estimations.

2. While the experiments agreed well with the computation for the IE-aerospike geometry, more resolution is required to confirm the delay of flow separation seen in the computational study.

3. At the flow conditions tested, the IE-aerospike produces a more favorable pressure field than the flared aerospike geometry; however, the flared aerospike design may be better suited to higher pressure ratio operation not tested in this study.

4. The relatively simplistic pressure model used for the computational study's RDE inflow boundary condition appears to produce results that agree well with the experiment.

Both the computational and experimental studies confirm that previous aerospike literature for constant pressure engines is not sufficient for estimating the nozzle performance for RDEs. On the computational side, performing full 3D transient studies modeling the combustion physics of the detonation wave would be useful to confirm the results from the more simplistic detonation wave pressure models. The study shown here only explores a small range of nozzle pressure ratios; more work into characterizing the flow physics for a greater range of pressure ratios will be required before design standards can be developed. At present, a new experimental RDE test campaign is under development at Purdue to explore higher area ratio nozzles suited for space engine applications. More pressure instrumentation will be included to gain better resolution of the surface pressures and a more detailed understanding of the nozzle flow physics.

References

[1] Lu, F. K. and Braun, E. M., "Rotating Detonation Wave Propulsion: Experimental Challenges, Modeling, and Engine Concepts," *Journal of Propulsion and Power*, Vol. 30, No. 5, Sept. 2014, pp. 1125-42. doi: 10.2514/1.B34802

[2] Stechmann, D. P., Heister, S. D., and Harroun, A. J., "Rotating Detonation Engine Performance Model for Rocket Applications," *Journal of Spacecraft and Rockets* (not yet published).

[3] Onofri, M., "Plug Nozzles: Summary of Flow Features and Engine Performance," 40th AIAA Aerospace Sciences Meeting and Exhibit, Reno, NV, Jan. 2002. doi: 10.2514/6.2002-584

[4] Hagemann, G., Immich, H., and Terhardt, M., "Flow Phenomena in Advanced Rocket Nozzles - The Plug Nozzle," 34th AIAA/ASME/SAE/ASEE Joint Propulsion Conference and Exhibit, Reston, VA, 1998. doi: 10.2514/6.1998-3522.

[5] Angelino, G., "Approximate Method for Plug Nozzle Design," *AIAA Journal*, Vol. 2, No. 10, 1964, pp. 1834-1835. doi: 10.2514/3.2682.

[6] Ishihara, K., et al., "Performance Evaluation of a Rotating Detonation Engine with Conical-Shape Tail," AIAA SciTech Forum, Kissimmee, FL, Jan. 2015. doi: 10.2514/6.2015-0630

[7] Harroun, A. J., "Investigation of Nozzle Performance for Rotating Detonation Rocket Engines," M.S. Thesis, Purdue University, July 2019.

[8] Stechmann, D. P., "Experimental Study of High-Pressure Rotating Detonation Combustion in Rocket Environments," Ph.D. Dissertation, Purdue University, 2017.

[9] Lim, D. and Humble, J., “Experimental Testing of an RP-2-GOX Rotating Detonation Rocket Engine,” AIAA SciTech Forum, Orlando, FL, Jan. 2020.
[10] Smith, S. D., “Final Report - Aerospike Design and Performance Tool," Plumetech, Huntsville, AL, Tech. Rep., August 2001, PT-FR-01-01.
[11] Gordon, S., McBride, B. J., "NASA Chemical Equilibrium with Applications," NASA Glenn Research Center.
[12] Mikoshiba, K., Sardeshmukh, S. V., and Heister, S. D., “Two Dimensional Simulation of RDE Combustor with a Dynamic Injection Model." AIAA SciTech Forum, San Diego, CA, Jan. 2019.
doi: 10.2514/6.2019-0477
[13] Luke, E. A., Tong, X. L., Wu, J., and Cinnella, P., “CHEM 2: A Finite-Rate Viscous Chemistry Solver -- The User Guide,” MSSU-COE-ERC-04-07, Mississippi State University, Sept. 2004.
[14] Roy, C. J., Tendean, E., Veluri, S. P., Rifki, R., Luke, E. A., Herbert, S., "Verification of RANS Turbulence Models in Loci-CHEM using the Method of Manufactured Solutions," 18th AIAA Computational Fluid Dynamics Conference, Miami, FL, June 2007.
[15] Mueller, T. J., Sule, W. P., Fanning, A. E., Giel, T. V., and Galanga, F. L., “Analytical and Experimental Study of Axisymmetric Truncated Plug Nozzle Flow Fields," National Aeronautics and Space Administration, Tech. Rep., Sept. 1972, NASA N-73-12282.
[16] Mueller, T. J., Sule, W. P., and Hall, C. R., “Characteristics of Separated Flow Regions within Altitude Compensating Nozzles," National Aeronautics and Space Administration, Tech. Rep., January, NASA N-71-18990.